Supporting Information for "Tracking Li atoms in real-time with ultra-fast NMR simulations"

Angela F. Harper[1], Tabea Huss[1], Simone S. Köcher[1,2], and Christoph Scheurer[1]
[1]*Fritz-Haber Institute of the Max Planck Society, Berlin (DE),* [2]*Institut für Energie und Klimaforschung (IEK-9), Forschungszentrum Jülich GmbH, Jülich, (DE)*

Appendix A: ML-EFG model hyperparameter optimization

All DFT calculations were performed with CASTEP v22.1 [1] using the C19 pseudopotential set and PBE exchange correlation functional [2]. The individual components of the EFG tensor, V_{ij}, were converged to within 4×10^{-3} V/Å^2 at a plane wave cutoff of 1200 eV and k-point spacing of $0.03\times2\pi$Å^{-1}. The ML-EFG approach uses λ-SOAP as the descriptor [3] which has hyperparameters l, n, r_c, and σ. These describe the number of angular components, number of radial components, cutoff radius, and Gaussian width of the descriptor. These hyperparameters were optimized using a combination of a Box-Behnken [4] design-of-experiment approach with 5-fold cross validation across a training set of 11,391 Li EFG tensors (80% of the total dataset). The optimal hyperparameters are $l = 6$, $n = 6$, $r_c = 6.0$ and $\sigma = 0.3$, which have a mean absolute error (MAE) of 7.4 kHz in ω_Q over the remaining 3057 Li environments (20% of the total data set) in the test set, which was withheld from cross validation. The MAE in C_Q and η is given in Figure S1. There is good Pearson correlation in both cases ($r > 0.85$) and low MAE (6.8 kHz MAE in C_Q and 0.99 MAE in η).

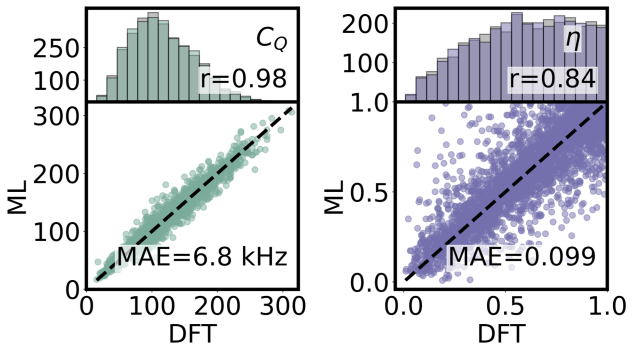

FIG. S1. **MAE over test set for C_Q and η** Histogram and correlation plot for C_Q and η evaluated over the 20% separated test set of 2057 Li environments in the ML-EFG model.

By testing the model using 11,391 Li EFG tensors on four additional large-scale structures withheld from training (results shown in Figure S2), we show that the ML-EFG model can be extended to the large LPS structures in our β-LPS and am-LPS simulations. The MAE in ω_Q over four large structures extracted from the UFP-MD trajectories is 9.2 kHz, which is within experimental accuracy of ^{7}Li SAE.

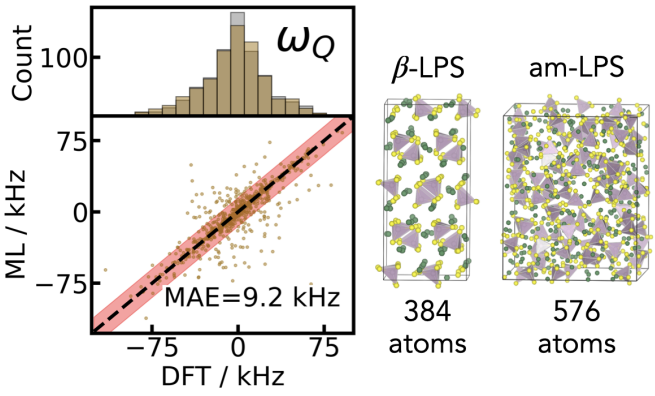

FIG. S2. **MAE in ω_Q for four large structures extracted from the UFP-MD trajectories** The left panel shows the MAE and distribution of ω_Q for a set of two β-LPS and two am-LPS structures extracted from the 1 μs UFP-MD simulations. Two of the structures are shown in the right panel, with PS_4 tetrahedra shown in purple (P) and yellow (S) and Li atoms shown in green.

Appendix B: Calculating autocorrelation functions

For all autocorrelation function calculations of β- and am-LPS, snapshots were extracted every 100 ps across the full trajectory. For the 1 μs calculations, this resulted in 10,000 total snapshots over which the ^{7}Li EFG tensors were predicted. The am-LPS structure has 576 atoms total with the stoichiometry Li_3PS_4, so there are a total of 216 Li atom trajectories in am-LPS over which the $\langle ACF_{\omega_Q}\rangle$ is averaged. For β-LPS there are 144 Li atoms, which $\langle ACF_{\omega_Q}\rangle$ is averaged over, and for $\langle ACF_{C_Q}\rangle$, the average is taken over only the Li ions which hop during the simulation (13 sites at 300 K and 102 sites at 350 K).

Both $\langle ACF_{\omega_Q}\rangle$ and $\langle ACF_{C_Q}\rangle$ were calculated using a sliding window averaging method in order to reduce the numerical noise between $\bar{\omega}_Q$ or $\bar{C}_Q$ at different timesteps, t_i. The sliding window average was 10 ns for $\langle ACF_{\omega_Q}\rangle$ and 1 ns for $\langle ACF_{C_Q}\rangle$. For the individual atom ACF_{C_Q} shown in Figures 5 and S3, the window was 10 ns to highlight the differences between LiS_4 and LiS_6. We can justify the validity of using the sliding window averaging through ergodicity, as averaging over a longer timescale is equivalent to averaging over a larger number of Li atoms at a fixed time. In addition, in order to account for the equilibration within the am-LPS structure, the initial $\omega_Q(t_0)$ used to reference the $\langle ACF_{\omega_Q}\rangle$ was taken as the average over the first 100 frames, or

$\langle \omega_Q(t_0), \omega_Q(t_1), ...\omega_Q(t_{100}) \rangle$. Finally, the $\langle \text{ACF}_{\omega_Q} \rangle$ is normalized between $[0, 1]$.

Appendix C: Simulations at 350 K

Given the slow diffusion time in β-LPS, there are a low number of hops (13 in total out of 144 Li atoms) at 300 K, and for that reason, we have included another trajectory at 350 K for β-LPS which has 102 hops in 1 μs. The corresponding hopping rate at 350 K is 1.70×10^6 s^{-1}, as extracted from the $\langle \text{ACF}_{C_Q} \rangle$ shown in Figure S3. This is an order of magnitude faster than for β-LPS at 300 K, which is the expected difference in hopping rates between these two temperatures.

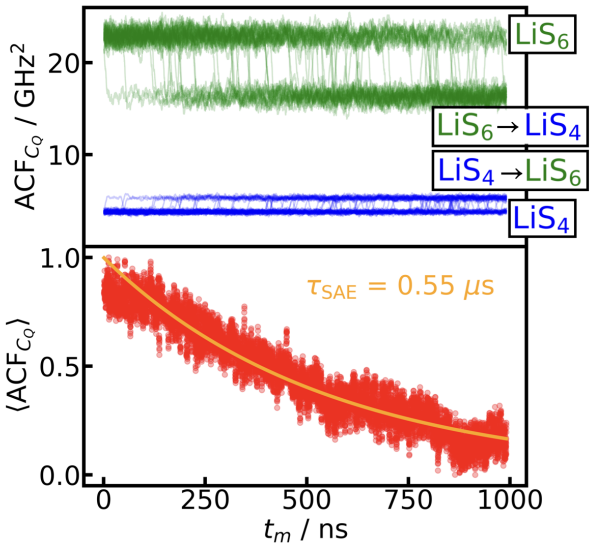

FIG. S3. **$\langle \text{ACF}_{C_Q} \rangle$ for β-LPS at 350 K** The calculated $\langle \text{ACF}_{C_Q} \rangle$ for a 1 μs trajectory of β-LPS at 350 K gives a decay rate of 0.59 μs or a Li hopping rate of 1.70×10^6 s^{-1}. Of the total 144 Li atoms in the cell, 102 atoms experienced a Li hopping event during the 1 μs simulation. The top panel distinguishes hopping events based on the initial site the Li atom was in at time $t = 0$. Initial LiS_6 sites (green) and initial LiS_4 sites (blue). The ACF_{C_Q} of each hopping event is labeled.

In addition to the $\langle \text{ACF}_{C_Q} \rangle$ over the 1 μs simulation, we also compare the angles θ and ϕ across the different sites in β-LPS in Figure S4. In the top panel, we find that for the Li atoms which remained in their original site, the angles (θ, ϕ) were centered around ($\pi/2$, 0) for LiS_4 tetrahedra and ($\pi/2\pm\pi/6$, $\pm\pi/4$) for LiS_6. For the Li sites which experience a hopping event at some point during the 1 μs simulation, we separate these into Li-ions which started out at a LiS_4 and LiS_6 site, respectively. As expected, the distribution of angles is wider for the hopping sites than for those that do not hop, but the majority of the hopping sites are LiS_6 sites which hop to another LiS_6 site. We can see this in the LiS_6 hop histogram (bottom right Figure S4) which has the highest density of (θ, ϕ) at ($\pi/2\pm\pi/6$, $\pm\pi/4$), which are all LiS_6 sites. Whereas, the LiS_4 hopping sites have a distribution of angles at both ($\pi/2\pm\pi/6$, $\pm\pi/4$), and ($\pi/2$, 0), indicating that some ions from LiS_4 sites hop into LiS_6 sites. However, all of these hopping events are masked in the $\langle \text{ACF}_{\omega_Q} \rangle$, as in Figure 3, and are only shown here in Figure S4 by decomposing the Li trajectories by their angular components.

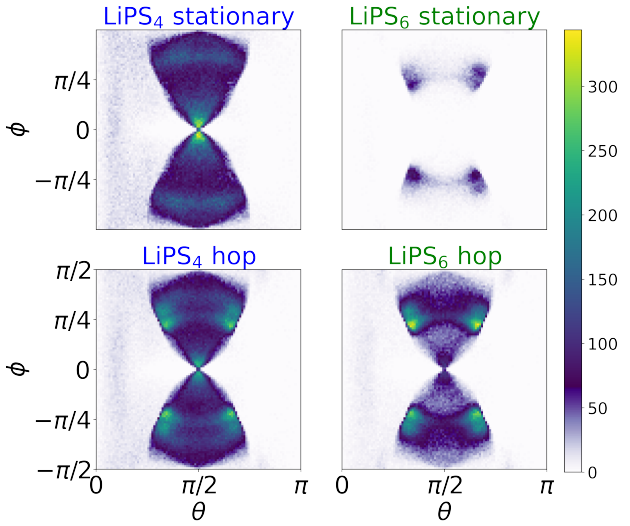

FIG. S4. **Distribution of θ and ϕ in β-LPS MD at 350 K separated by local environment.** The four heatmaps show, qualitatively, the different angular environments accessed during the 1 μs simulation for sites which do not experience a hopping event (top) and sites which do experience a hopping event (bottom) starting from either an LiS_4 or LiS_6 site. The histograms are colored by the number of Li sites across the trajectory which have a given (θ,ϕ).

Appendix D: Technical details of the UFP fitting

The UFP-MD simulations for training are executed at temperatures ranging from 300 K to 1000 K, using a time step of 2 fs, and a simulation time of either 1 ns or 1 μs in the NpT ensemble. All DFT reference calculations used for generating the UFP are performed using FHI-AIMS [5], the PBE exchange-correlation functional [6] and a 2×2×2 k-point sampling. Hyperparameter optimization was performed and the results are shown in Table I. The RDFs of β-LPS and am-LPS compared to AIMD from [7, 8] are shown in Figure S5.

Finally, to compare the atom dynamics in the UFP versus another high quality machine learning potential for LPS, we simulated a 1 ns trajectory at 500 K for both β- and am-LPS using the UFP [9] and TurboGAP [10]. The resulting MSDs are shown in Figure S6, and we find that for am-LPS the MSD is comparable between TurboGAP and the UFP, and for β-LPS we have a five times faster transport in the TurboGAP compared to UFP. This can be explained by a insufficient barrier sampling in the approaches, as the fitting of the interatomic potentials is done using snapshots from MD simulations. Those snap-

TABLE I. **Hyperparameters of the UFP**

Description	2B	3B
cutoff	6 Å	5 Å
lower cutoff	1 Å	1 Å
spline distance	0.4 Å	0.4 Å
ridge regularisation	1e-5	1e-6
curvature regularisation	1e-5	1e-5
κ	0.1	
leading trim	0	
trailing trim	3	

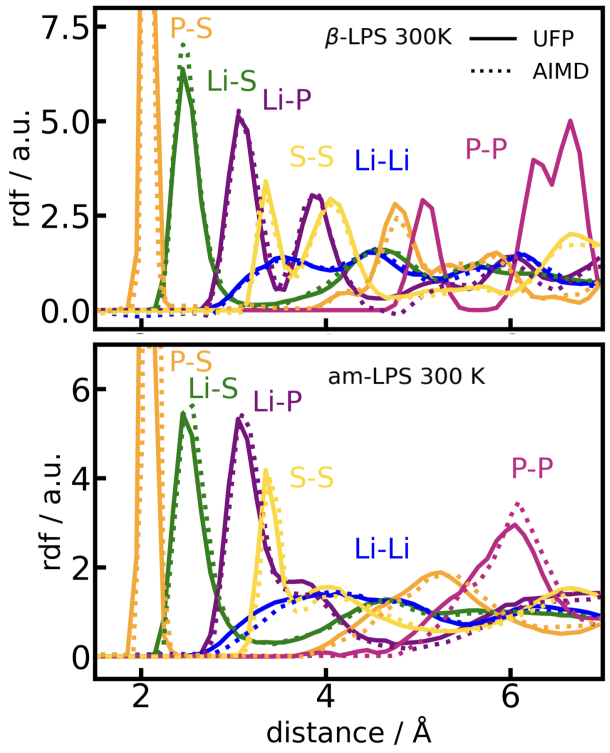

FIG. S5. **Radial distribution functions of β-LPS and am-LPS in comparison to AIMD references**. β-LPS (top) is compared to the AIMD RDF from Sadowski *et al.* [7] and am-LPS (bottom) to the AIMD RDF from Smith *et al* [8].

shots are strongly biased towards the minima and a better estimate of the barrier height could be achieved by including nudged elastic band [11] trajectories from DFT into the training sets of both MLIPs.

Appendix E: Technical details of jump detection

For the discretization in order to detect jumps, we utilize a hopping classification inspired by Smith *et al.* [8],

$$h_i(t, a) = \theta(|r_i(t) - r_i(t_0)| - a), \tag{S1}$$

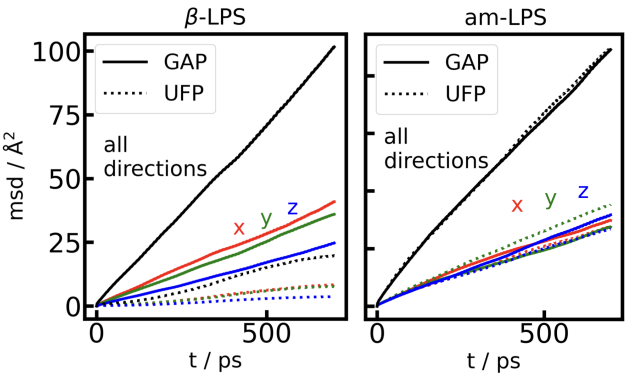

FIG. S6. **Mean square displacement of a 1 ns MD run of β-LPS and am-LPS at 500 K** The MSD for β-LPS (left) and am-LPS (right) is compared between 1 ns simulations in TurboGAP [10] and UFP [9] in order to validate the Li diffusion behavior in the UFP model.

where θ is the Heaviside function and a is a threshold of square displacement. We set a to 3 Å and provide a sensitivity analysis for this parameter (Figure S7). The hopping detection method, Equation S1, is run over a single Li trajectory until a hop is detected, and then repeated iteratively, using the detected hopping point as a new starting point. Also an additional filter is used which ensures a residence time of 0.5 ns to exclude jump attempts from the detection. Examples of discretized Li squared displacement trajectories of the β-LPS are shown in Figure 2 (right).

We test the sensitivity of the calculated jump frequency from MD simulations on the selected threshold a from Equation S1 and show the result in Figure S7. We find a plateau between 2.8 and 3.2 Å and thus select a cutoff of 3 Å.

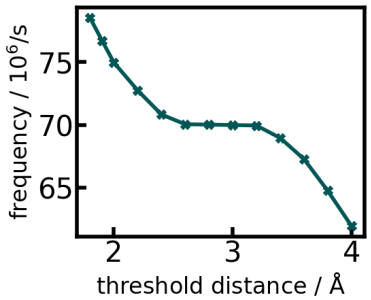

FIG. S7. **Sensitivity of the computed jump frequency on the selected threshold a of the absolute displacement for am-LPS** By varying the threshold distance, a for computing a jump frequency we find a window in which the jump frequency is stable (between 2.8 and 3.2 Å) and use this to select the optimal threshold distance, 3.0 Å.

[1] S. J. Clark, M. D. Segall, C. J. Pickard, P. J. Hasnip, M. I. Probert, K. Refson, and M. C. Payne, First principles methods using CASTEP, Z. Kristallogr. Cryst. Mater. **220**, 567 (2005).

[2] J. P. Perdew, K. Burke, and M. Ernzerhof, Generalized gradient approximation made simple, Phys. Rev. Lett. **77**, 3865 (1996).

[3] A. Grisafi, D. M. Wilkins, G. Csányi, and M. Ceriotti, Symmetry-adapted machine learning for tensorial properties of atomistic systems, Physical Review Letters **120**, 036002 (2018).

[4] G. E. Box and N. R. Draper, *Empirical model-building and response surfaces.* (John Wiley & Sons, 1987).

[5] V. Blum, R. Gehrke, F. Hanke, P. Havu, V. Havu, X. Ren, K. Reuter, and M. Scheffler, Ab initio molecular simulations with numeric atom-centered orbitals, Computer Physics Communications **180**, 2175 (2009).

[6] J. P. Perdew, K. Burke, and M. Ernzerhof, Generalized gradient approximation made simple, Physical Review Letters **77**, 3865 (1996).

[7] M. Sadowski and K. Albe, Computational study of crystalline and glassy lithium thiophosphates: Structure, thermodynamic stability and transport properties, Journal of Power Sources **478**, 229041 (2020).

[8] J. G. Smith and D. J. Siegel, Low-temperature paddle-wheel effect in glassy solid electrolytes, Nature Communications **11**, 10.1038/s41467-020-15245-5 (2020).

[9] S. R. Xie, M. Rupp, and R. G. Hennig, Ultra-fast interpretable machine-learning potentials, npj Computational Materials **9**, 162 (2023).

[10] M. A. Caro, Optimizing many-body atomic descriptors for enhanced computational performance of machine learning based interatomic potentials, Physical Review B **100**, 024112 (2019).

[11] H. Jónsson, G. Mills, and K. W. Jacobsen, Nudged elastic band method for finding minimum energy paths of transitions, in *Classical and Quantum Dynamics in Condensed Phase Simulations* (World Scientific, 1998).